

## Computerized Scheme for Detection of Arterial Occlusion in Brain MRA Images

Masashi Yamauchi\*<sup>a</sup>, Yoshikazu Uchiyama<sup>a</sup>, Ryujiro Yokoyama<sup>a</sup>, Takeshi Hara<sup>a</sup>, Hiroshi Fujita<sup>a</sup>,  
Hiromichi Ando<sup>b</sup>, Hiroyasu Yamakawa<sup>c</sup>, Toru Iwama<sup>d</sup>, Hiroaki Hoshi<sup>e</sup>

<sup>a</sup> Department of Intelligent Image Information, Graduate School of Medicine, Gifu University.,  
Yanagido 1-1, Gifu 501-1194, Japan

<sup>b</sup> Department of Neurosurgery, Gifu Municipal Hospital, Kashima 7-1, Gifu 500-8323, Japan

<sup>c</sup> Department of Emergency and Critical Care Medicine, Chuno-Kousei Hospital, Wakakusadori 5-1,  
Seki 501-3802, Japan

<sup>d</sup> Department of Neurosurgery, Graduate School of Medicine, Gifu University., Yanagido 1-1, Gifu  
501-1194, Japan

<sup>e</sup> Department of Radiology, Graduate School of Medicine, Gifu University, Yanagido 1-1, Gifu  
501-1194, Japan

### ABSTRACT

Magnetic resonance angiography (MRA) is routinely employed in the diagnosis of cerebrovascular disease. Unruptured aneurysms and arterial occlusions can be detected in examinations using MRA. This paper describes a computerized detection method of arterial occlusion in MRA studies. Our database consists of 100 MRA studies, including 85 normal cases and 15 abnormal cases with arterial occlusion. Detection of abnormality is based on comparison with a reference (normal) MRA study with all the vessel known. Vessel regions in a 3D target MRA study is first segmented by using thresholding and region growing techniques. Image registration is then performed so as to maximize the overlapping of the vessel regions in the target image and the reference image. The segmented vessel regions are then classified into eight arteries based on comparison of the target image and the reference image. Relative lengths of the eight arteries are used as eight features in classifying the normal and arterial occlusion cases. Classifier based on the distance of a case from the center of distribution of normal cases is employed for distinguishing between normal cases and abnormal cases. The sensitivity and specificity for the detection of abnormal cases with arterial occlusion is 80.0% (12/15) and 95.3% (81/85), respectively. The potential of our proposed method in detecting arterial occlusion is demonstrated.

**Keywords:** Computer-aided diagnosis, Magnetic resonance angiography, Arterial occlusion, Image registration

### 1. INTRODUCTION

Cerebrovascular disease is the third cause of death in Japan [1]. The prevention of such disease has been receiving great attentions. Magnetic resonance imaging (MRI) and magnetic resonance angiography (MRA) are very useful for the early detection of cerebral and cerebrovascular diseases and are widely used in a health check system named *Brain Dock* in Japan. Asymptomatic lacunar infarct, unruptured aneurysm, and arterial occlusion are often detected in the examination with MRI and MRA studies. Therefore, we have been developed computer-aided diagnosis (CAD) schemes for detection of these diseases in brain MR images [2-4] in order to assist radiologists' diagnosis as a "second opinion" in the *Brain Dock*.

The presence of asymptomatic lacunar infarcts increases the risk of serious cerebral infarction. Thus, it is important

---

Corresponding author information: E-mail: [masashi@fjt.info.gifu-u.ac.jp](mailto:masashi@fjt.info.gifu-u.ac.jp), Telephone: +81-58-230-6519

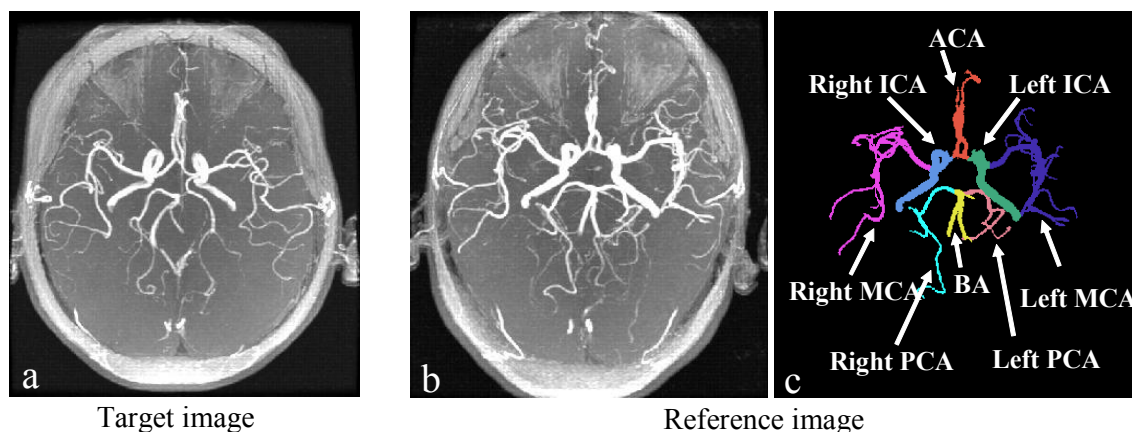


Fig. 1 Target image and reference image. (a) A MIP image of Target image. The target image was changed to register the reference image. (b) A MIP image of the Reference image. (c) The eight pre-labelled arteries showed on the reference image in (b).

to detect lacunar infarcts in MRI images. However, it is hard for radiologists and/or neurosurgeons to identify lacunar infarcts in MRI images because of the difficulty for distinguishing between lacunar infarcts and normal tissues such as Virchow-Robin spaces. Our previous study on CAD scheme for detection of lacunar infarcts in T1- and T2- weighted images has been reported [2]. The detection of unruptured aneurysms in MRA studies is also an important task for radiologists because the rupture of aneurysms is the major cause of subarachnoid haemorrhage (SAH). However, it is difficult to detect small aneurysms in MRA studies because of the overlapping of aneurysms and adjacent vessels on maximum intensity projection (MIP) image. A number of CAD schemes for detection of aneurysms in MRA studies have been proposed [3-7]. These studies showed that CAD can improve neuroradiologists and general radiologists in detecting intracranial aneurysms with MR angiography [8]. Although some studies have reported on CAD schemes for detection of lacunar infarcts and aneurysms, there have been no reports on the detection of arterial occlusion in MRA studies.

In facilitating the radiologists in detecting small aneurysms, we developed a *SelMIP* image as a new viewing technique in our CAD scheme [4]. The technique takes on an approach in making a new type of MIP image with interested vessel regions only by manually selecting a desired cerebral artery from a list. By using our new viewing technique, the selected vessel region can be observed from various directions, and small aneurysms would be easy to detect. In this technique, we developed a new method for automated labeling of eight arteries in MRA studies. By using this method, we can calculate the length of eight arteries. The length of vessel with arterial occlusion is short in comparison with the normal vessel. Thus, we can distinguish between normal cases and abnormal case with arterial occlusion by using the lengths of arteries as features. This paper describes a CAD scheme for detection of arterial occlusion in MRA studies based on the relative length of eight arteries.

## 2. MATERIAL

A database consists of 100 MRA studies, including 85 normal and 15 abnormal with arterial occlusion, was collected. Sixteen of the MRA studies were acquired on a 1.5 T magnetic image scanner (a Signa Excite Twin Speed 1.5T; GE Medical System) at the Gifu University Hospital (Gifu, Japan). Each of these MRA studies includes 50 to 140 slice images. The axial slice images have a fixed size of 256×256 pixels and the size of the pixels ranges from 0.625 mm to 0.78 mm. The thickness of each slice is in the range of 0.5 mm to 1.2 mm. The remaining 84 MRA studies were acquired on a 1.5 T magnetic image scanner (Symphony; SIMENS) at the Gero Hot Springs Hospital (Gero, Japan). Each MRA study includes 72 to 80 slice images. The axial slice images have a size of either 256×192 or 256×176 pixels. Despite the slight variation in the image size, the axial slice images in all 84 cases have the same pixel size and slice thickness of 0.7mm and 1mm, respectively. In addition, a reference (normal) MRA study was also acquired on the above mentioned magnetic image scanner at the Gifu University Hospital using the same image acquisition parameters. All 100

studies and the reference study were obtained by use of a 3D time-of-flight technique. The acquired MRA data were subsequently converted to isotropic volume data by using linear interpolation. The size of the converted 3D volume data is  $400 \times 400 \times 200$  voxels, whereas the size of each voxel is  $0.5 \times 0.5 \times 0.5 \text{mm}^3$ . The isotropic volume data were employed in all experimental work in this study.

### 3. METHODOLOGY

#### 3.1 Overall scheme for automated detection of arterial occlusion

Our scheme for automated detection of arterial occlusion consists of two parts, i.e., (1): classification of eight arteries, and (2): detection of arterial occlusion based on relative lengths of eight arteries. For the classification of arteries, the 3D reference image was used as a reference for the locations of eight arteries to be segmented in all MRA studies. The eight cerebral arteries were pre-labeled in the 3D reference image. They are the anterior cerebral artery (ACA), right middle cerebral artery (MCA), left middle cerebral artery, right internal carotid artery (ICA), left internal carotid artery, right posterior cerebral artery (PCA), left posterior cerebral artery, and basilar artery (BA). Image registration was performed on the 3D reference image and an image to be classified, referred to as a target image, with the former kept unchanged. Fig.1 shows a target image and a reference image. Segmentation of the vessel regions was subsequently performed by using the thresholding and region growing techniques. The segmented vessel regions in the target image were then shifted to align with the reference image by using a global matching procedure and rigid transformation. Recognition of each of the cerebral arteries was based on the Euclidean distance measured between a labeled artery in the reference image and the segmented vessel pixels in the target image. For the detection of arterial occlusion, the lengths of the eight arteries in the classified vessel regions were calculated. A classifier using the relative lengths of the arteries as features was employed in distinguishing between normal case and abnormal case with arterial occlusion.

#### 3.2 Segmentation of vessel region

For the segmentation of the vessel regions in the target image, a linear gray-level transform was applied to the 3-dimensional MRA image so that the minimum voxel value became zero, and voxels with values above the 99% margin depicted in a cumulative histogram were assigned to a maximum value of 1024. After the linear gray-level transformation, vessel regions were segmented from the background by using the gray-level thresholding method with a threshold level of 700, which was selected empirically. Using this method, the regions of large vessels were segmented successfully. However, it is difficult to segment small vessels using this method because the voxel values in small vessel regions were low. A region growing technique was subsequently applied to segment the small vessel regions. The segmented large vessel regions were used as "seed" points and neighboring voxels with values greater than 500 were appended to the seed points.

#### 3.3 Global matching

As the locations of the corresponding vessel regions in the target image and the reference image are likely to be different due to variation in patient positioning, registration of the corresponding vessel regions is necessary. Global matching was used in the initial image registration. In the global matching procedure, the translation vector was defined so as to maximize the overlapping of the vessel regions in the target image and the reference image. By using the global matching technique, the corresponding vessel regions in the two images were brought close to each other.

#### 3.4 Corresponding control points

After the global matching procedure, the rigid transformation [9] was used to achieve a more accurate matching between the target image and the reference image. A number of control points were pre-determined in the reference image and the template matching method was used to determine the locations of the corresponding control points in the target image. In the template matching procedure, the normalized cross-correlation value,  $C$ , was used as a similarity measure. The normalized cross-correlation value,  $C$ , between the template  $A$ , containing a pre-determined feature point on the reference image, and a region  $B$ , containing a candidate corresponding feature point on the target image is given by

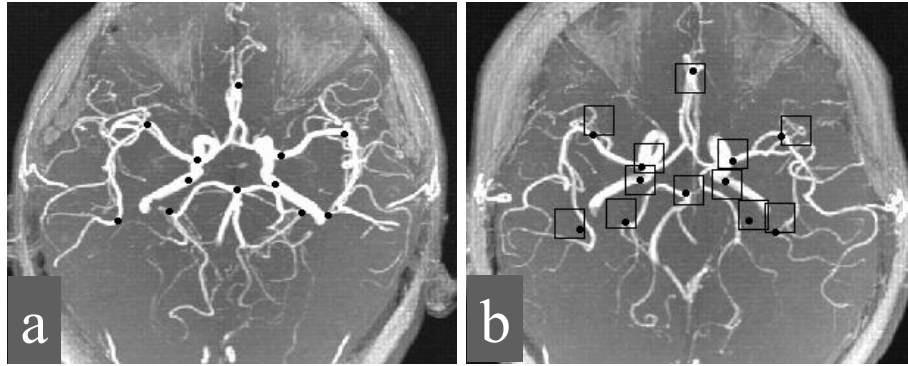


Fig. 2 Corresponding control points for the rigid transformation. (a) The center points of the 12 templates (black dots) projected onto the MIP image of the reference MRA study. (b) Corresponding points (black dots) in the MIP image of the target MRA study was found using the template matching method. Square boxes indicate the search areas for individual control points.

$$C = \frac{1}{IJK} \sum_{k=1}^K \sum_{j=1}^J \sum_{i=1}^I \frac{\{A(i, j, k) - \bar{a}\} \{B(i, j, k) - \bar{b}\}}{\sigma_A \sigma_B} \quad (1)$$

where

$$\bar{a} = \frac{1}{IJK} \sum_{k=1}^K \sum_{j=1}^J \sum_{i=1}^I A(i, j, k), \quad (2)$$

$$\bar{b} = \frac{1}{IJK} \sum_{k=1}^K \sum_{j=1}^J \sum_{i=1}^I B(i, j, k), \quad (3)$$

$$\sigma_A = \sqrt{\frac{\sum_{k=1}^K \sum_{j=1}^J \sum_{i=1}^I (A(i, j, k) - \bar{a})^2}{IJK}}, \quad (4)$$

$$\sigma_B = \sqrt{\frac{\sum_{k=1}^K \sum_{j=1}^J \sum_{i=1}^I (B(i, j, k) - \bar{b})^2}{IJK}}. \quad (5)$$

The size of the template  $I \times J \times K$  was set to be  $21 \times 21 \times 21$ . The normalized cross-correlation value indicates the resemblance between the reference and the template. If the images  $A$  and  $B$  are identical,  $C$  will take on the value 1.0. Twelve templates were located manually in the cerebral region of the reference image. Fig.2 (a) shows the center points of the twelve templates in black dots. The search region associates with each template in the target image was of size  $41 \times 41 \times 41$ . A set of coordinates of the corresponding points between the reference and the target image was determined by finding the largest cross-correlation value. Fig.2 (b) shows the twelve corresponding points found in the target image using the template matching method.

### 3.5 Rigid transformation of the target image

By using a set of corresponding control points determined by the template matching method, the translation and rotation vectors,  $T$  and  $R$ , between the two images for the rigid transformation were determined. Let  $P$  and  $p$  represent the corresponding points in the reference and the target images, respectively. Assuming the coordinates of the corresponding points in the images after global matching are  $\{p_i = (x_i, y_i, z_i), P_i = (X_i, Y_i, Z_i): i = 1, \dots, 12\}$ , the relation between the corresponding points in the images can be written as

$$P_i = R p_i + T. \quad (6)$$

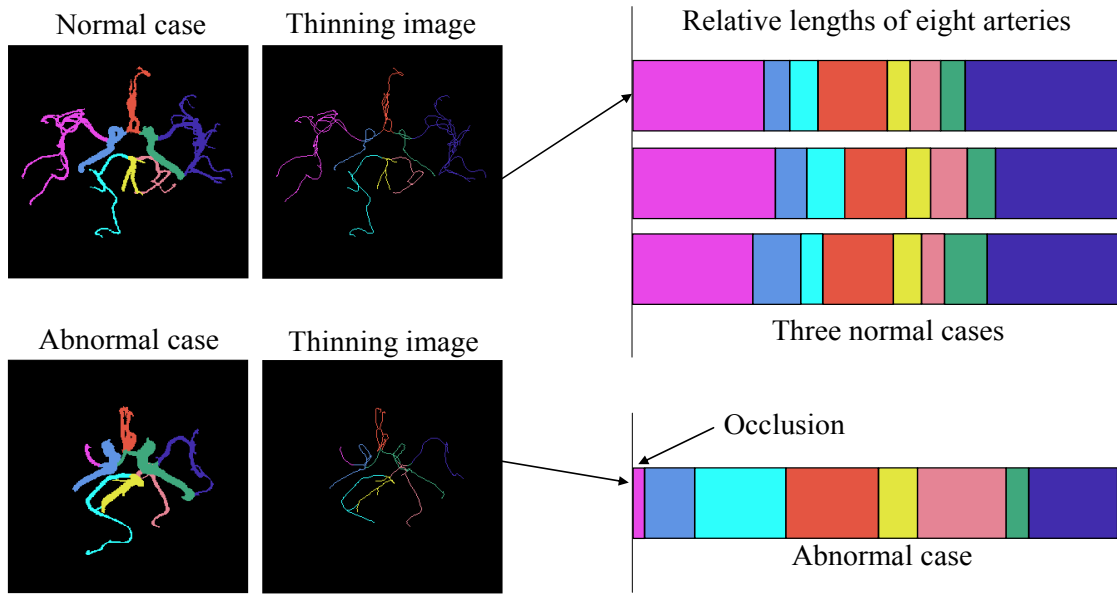


Fig.3 Relative lengths of the eight arteries obtained from three normal cases and an abnormal case with arterial occlusion.

The translation vector  $T$  and the rotation vector  $R$  can be determined by minimizing

$$E^2 = \sum_{i=1}^p \|P_i - (Rp_i + T)\|^2. \quad (7)$$

An efficient algorithm has proposed for determining  $T$  and  $R$  [10]. In this algorithm, the rotation matrix is obtained first by minimizing

$$E_r^2 = \sum_{i=1}^p \|Q_i - R_i q_i\|^2, \quad (8)$$

where  $Q_i = P_i - \bar{P}$ ,  $q_i = p_i - \bar{p}$ , and  $\bar{P}$  and  $\bar{p}$  are the centers of gravity of the control points in the reference and target image, respectively. Then, knowing the rotation matrix, the translation vector  $T$  is determined from

$$T = P - Rp. \quad (9)$$

For calculating the closest corresponding point pairs, the iterative closest point (ICP) algorithm [11, 12] was used. The ICP algorithm has two iterative stages. In the first stage, the set of corresponding points was transformed by using the rigid transformation in Eq. (6). In the second stage, the closest corresponding point pairs were identified once again for the next rigid transformation. The algorithm iterates until the change in mean square error between iterations fell below a defined threshold.

### 3.6 Classification of cerebral arteries

After the rigid transformation, all voxles in the segmented vessel regions of the target image were classified into eight cerebral arteries. Classification was based on the Euclidean distance between a voxel  $v(x, y, z)$  in the target image and a voxel  $a^i(x^i, y^i, z^i)$ ,  $\{i = 1, \dots, 8\}$  in the labeled eight vessel regions in the reference image, i.e.,

$$d(v, a^i) = \sqrt{(v_x - a_x^i)^2 + (v_y - a_y^i)^2 + (v_z - a_z^i)^2}. \quad (10)$$

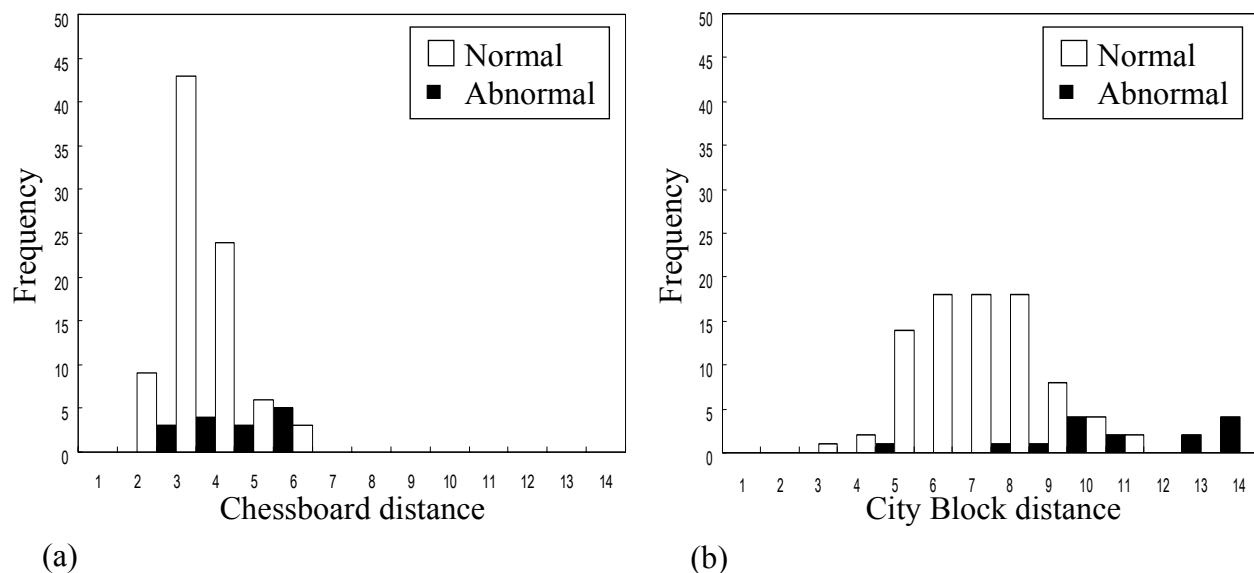


Fig. 4 Histograms of distance for distinction between normal cases and abnormal cases. (a) Chessboard distance. (b) City Block distance.

The classification result yielding the minimum Euclidean distance was considered to be the best initial result. A few small regions may not be classified correctly at this stage because of the slight deviation in vessels lengths and locations in individual cases. To rectify the potential miss classification, the label of the largest component in each of the eight labels were kept unchanged, whereas the rest of the regions were re-labelled based on their distances from the above eight labeled components.

### 3.7 Detection of arterial occlusion based on relative length of arteries

In order to eliminate the effect of the thickness of vessels, 3D thinning transformation [13, 14] was applied to the labeled vessel regions. The absolute lengths of the eight arteries were obtained by counting the total number of labeled voxels. The lengths of the eight arteries were found to be different in different MRA studies. However, the relative lengths of the eight arteries were similar among normal cases. The relative length of an artery,  $RL_i$ , is defined as

$$RL_i = L_i / TL \quad i = 1, \dots, 8, \quad (11)$$

where  $L_i$  is the length of one of the  $i$ th labeled arteries.  $TL$  is the total length of the eight labeled arteries. Fig. 3 shows the relative lengths of the eight arteries obtained from three normal cases and an abnormal case with arterial occlusion. As shown in the figure, the relative lengths of the eight arteries obtained from the normal cases are similar. However, the relative lengths of the eight arteries obtained from the abnormal case are quite different from those obtained from the normal cases because the length of artery with occlusion is shortened. In building the classification in detecting arterial occlusion the relative lengths of the eight arteries are used as eight features. The features were then normalized by using the average values and the standard deviations of the eight features obtained from the normal cases. In the feature space, the distribution of eight features for normal cases was centered around the origin, whereas the distribution of eight features for abnormal cases was generally shifted from the origin. The distance from the origin indicates the likelihood of abnormality. A classifier based on the distance of a case from the origin was employed for the detection of abnormal cases with arterial occlusion.

In order to calculate the distance from the origin, three types of distance were investigated, i.e., Euclidean distance, Chessboard distance, and City Block distance [15]. The Euclidean distance,  $D_e$ , is known from classical geometry and the distance between two points with co-ordinates  $(i, j, k)$  and  $(l, m, n)$  is defined as

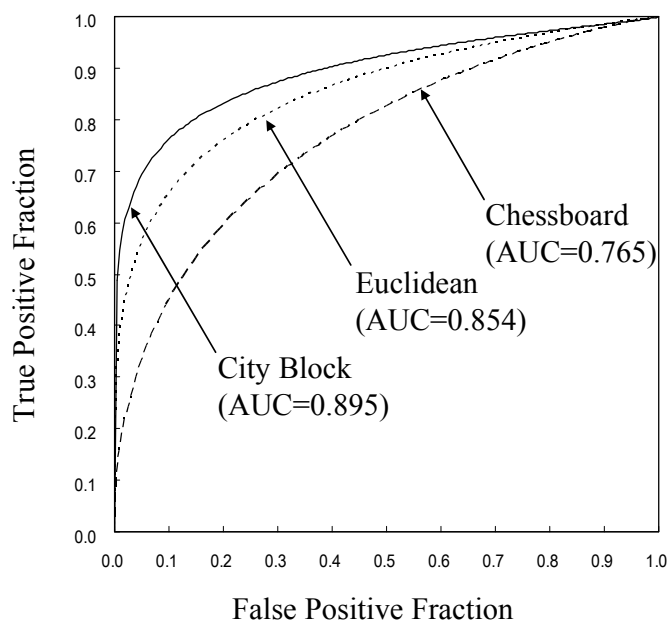


Fig. 5 ROC curves for distinction between normal cases and abnormal cases with arterial occlusion by using the City Block distance, Euclidean distance, and Chessboard distance, respectively.

$$D_e[(i, j, k), (l, m, n)] = \sqrt{(i-l)^2 + (j-m)^2 + (k-n)^2} . \quad (12)$$

The Chessboard distance,  $D_8$ , is equal to the number of moves of the king on the chessboard from one part to another, which is given as

$$D_8[(i, j, k), (l, m, n)] = \max\{|i-l|, |j-m|, |k-n|\} . \quad (13)$$

The pixels with  $D_8 = 1$  are the 8-neighbors of the point located at  $(i, j, k)$ . The City Block distance,  $D_4$ , is defined as

$$D_4[(i, j, k), (l, m, n)] = |i-l| + |j-m| + |k-n| . \quad (14)$$

The name ‘City Block’ was coined because of the analogy with the distance between two locations in a city with a rectangular grid of streets and closed blocks of houses. The pixels with  $D_4 = 1$  are the 4-neighbors of  $(i, j, k)$ .

#### 4. RESULTS AND DISCUSSIONS

The proposed method was evaluated by applying to 100 MRA studies, consisting of 85 normal cases and 15 abnormal cases with arterial occlusion. Vessel regions in MRA images were first segmented. The segmented vessel regions were then classified into eight arteries. The relative lengths of the eight arteries were determined and were used in distinguishing normal cases and abnormal cases with arterial occlusion. The features were normalized by using the average values and the standard deviations of the eight features obtained from the normal cases. Finally, a case was classified as normal or abnormal based on the distance measure of the case from the origin in the feature space. Fig. 4 shows histograms obtained from the normal cases and the abnormal cases using the Chessboard distance measure and the City Block distance measure, respectively. When using the Chessboard distance, discrimination between the normal cases and the abnormal cases is difficult because the distribution of the normal cases overlapped with that of the abnormal cases. However, in the case of the City Block distance, some abnormal cases could be clearly distinguished from the normal cases.

To evaluate the performance of our CAD scheme using the Chessboard distance, the Euclidean distance, and the City Block distance, ROC analysis was used [16, 17]. The distances obtained from the normal cases and the abnormal cases

were used as decision scores in the ROC analysis. Binormal distributions were fitted to the scores by use of maximum-likelihood estimation [17]. The ROC curve was obtained by changing the threshold value in the distribution of the distances obtained from output value of CAD scheme. Fig. 5 shows the ROC curves obtained from CAD schemes using the Chessboard distance, the Euclidean distance, and the City Block distance, respectively. The AUC values (area under the ROC curve) for Chessboard distance, Euclidean distance and City Block distance were 0.765, 0.854, and 0.895, respectively. The results indicate that the CAD scheme based on City Block distance achieved the best performance. As the result, with the CAD scheme based on City Block distance, the sensitivity and specificity for the detection of abnormal cases with arterial occlusion were 80.0% (12/15) and 95.3% (81/85), respectively.

## 5. CONCLUSION

We developed a computerized method for detection of abnormal cases with arterial occlusions. The sensitivity and specificity for distinction between normal cases and abnormal cases with arterial occlusions were 80.0% (12/15) and 95.3% (81/85) with AUC of 0.895 under the ROC curve. Therefore, our computerized method might be useful for automatic detection of abnormal cases with arterial occlusion in MRA studies.

## ACKNOWLEDGMENT

This work was supported in part by a grant for the “Knowledge Cluster Creation Projection” from the Ministry of Education, Culture, Sports, Science and Technology Japan. The authors thank Hitoshi Futamura, Akiko Kano, and Hitoshi Yoshimura of Konica Minolta Medical & Graphic, Inc. and Yoshinori Hayashi and Masakatsu Kakogawa of TAK CO. Ltd. for their valuable suggestions. The authors also thank the members of Fujita Laboratory in the Department of Intelligent Image Information, Graduate School of Medicine, Gifu University.

## REFERENCES

1. Health and Welfare Statistics Association, “Vital Statistics of Japan 2003,” volume 1, 2003.
2. Y. Uchiyama, A. Matsui, R. Yokoyama, H. Fujita, H. Hara, X. Zhou, H. Ando, T. Iwama, T. Asano, H. Kato, and H. Hoshi, “CAD scheme for detection of lacunar infarcts in brain MR image,” *International Journal of Computer Assisted Radiology and Surgery*, 1(1), 382-385, 2006.
3. Y. Uchiyama, H. Ando, R. Yokoyama, T. Hara, H. Fujita, and T. Iwama, “Computer-Aided Diagnosis Scheme for Detection of Unruptured Intracranial Aneurysms in MR Angiography,” *Proc of IEEE Engineering in Medicine and Biology 27<sup>th</sup> Annual International Conference*, Shanghai, China, 3031-3034, 2005.
4. Y. Uchiyama, M. Yamauchi, H. Ando, R. Yokoyama, T. Hara, H. Fujita, T. Iwama, and H. Hoshi, “Automated classification of cerebral arteris in MRA images and its application to maximum intensity projection,” *Proc of IEEE Engineering in Medicine and Biology 28<sup>th</sup> Annual International Conference*, New York, USA, 4865-4868, 2006.
5. H. Arimura, Q. Li, Y. Korogi, T. Hirai, H. Abe, Y. Yamashita, S. Katsuragawa, R. Ikeda, and K. Doi, “Automated computerized scheme for detection of unruptured intracranial aneurysms in three-dimensional MRA,” *Academic Radiology*, 11(10), 1093-1104, 2004.
6. H. Arimura, Q. Li, Y. Korogi, T. Hirai, S. Katsuragawa, Y. Yamashita, K. Tsuchiya, and K. Doi, “Computerized detection of intracranial aneurysms for three-dimensional MR angiography: Feature extraction of small protrusions based on a shape-based difference image technique,” *Medical Physics*, 33(2), 394-401, 2006.
7. N. Hayashi, Y. Masutani, T. Matsumoto, H. Mori, A. Kunimatsu, O. Abe, S. Aoki, K. Ohtomo, N. Takano, and K. Matsumoto, “Feasibility of a curvature-based enhanced display system for detecting cerebral aneurysms in MR angiography,” *Magnetic Resonance in Medical Science*, 2, 29-36, 2003.
8. T. Hirai, Y. Korogi, H. Arimura, S. Katsuragawa, M. Kitajima, M. Yamura, Y. Yamashita, and K. Doi, “Intracranial aneurysms at MR angiography: effect of computer-aided diagnosis on radiologists’ detection performance,” *Radiology*, 237, 605-610, 2006
9. A. A. Goshtasby, “2-D and 3-D image registration,” *John Wiley & Sons, Inc.*. Hoboken, New Jersey, 2005.
10. K. S. Arum, T. S. Huang, and S. D. Blostein, “Least-square fitting of two 3-D point sets,” *IEEE Trans. on Pattern Analysis and Machine Intelligence*, 9(5), 698-700, 1987.

11. P. J. Besl and N. D. McKay, "A method for registration of 3-D shapes," *IEEE Trans. on Pattern Analysis and Machine Intelligence*. 14(2), 239-256, 1992.
12. J. Feldmar, J. Declerck, G. Malandain, and N. Ayache, "Extension of the ICP algorithm to nonrigid intensity-based registration of 3-D volumes," *Computer Vision and Image Understanding*. 66(2), 193-206, 1997.
13. T. Saito and J. Toriwaki, "A sequential thinning algorithm for three dimensional digital pictures using the Euclidean distance transform," Proc. of 9<sup>th</sup> SCIA(*Scandinavia Conf. o Image Analysis*), 507-516, 1995.
14. T. Saito and J. Toriwaki, "New algorithms for Euclidean distance transformations of an n-dimensional digitized picture with applications," *Patten Recognition*, 27, 1551-1565, 1994 .
15. R. G. Gonzalez and R. E. Woods, "Digital Image Processing," Addison-Wesley, Boston, MA, 1993.
16. C. E. Metz, J. H. Shen, and B. A. Herman, "New method for estimating a binormal ROC curve from continuously-distributed test results," *Annual Meeting of the American Statistical Association*, Anaheim, CA, 1990.
17. C. E. Metz, J. H. Shen, and B. A. Herman, "Maximum likelihood estimation of receiver operation characteristic (ROC) curve from continuously-distributed data," *Statistics in Medicine*. 17, 1033-1053, 1998.